Larkin-Ovchinnikov superfluidity in a two-dimensional imbalanced atomic Fermi gas

Umberto Toniolo,[*] Brendan Mulkerin, Xia-Ji Liu, and Hui Hu

Centre for Quantum and Optical Science, Swinburne University of Technology, Hawthorn 3122 VIC, Australia
(Received 22 September 2016; published 4 January 2017)

We present an extensive study of two-dimensional Larkin-Ovchinnikov (LO) superfluidity in a spin-imbalanced two-component atomic Fermi gas. In the context of Fulde-Ferrell-Larkin-Ovchinnikov (FFLO) phase, we explore a wide and generic class of pairing gap functions with explicit spatial dependency. The mean-field theory of such phases is applied through the Bogoliubov-de Gennes equations in which the pairing gap can be determined self-consistently. To systematically explore the configuration space we consider both the canonical and grand canonical ensembles where we control the polarization or chemical potentials of the system, respectively. The mean-field calculations enable us to understand the nature of the phase transitions in the fully paired Bardeen-Cooper-Schrieffer (BCS) state, exotic LO phase, and partially polarized free Fermi gas (N_{PP}). The order of the phase transitions has been examined and, in particular, we find a weak first-order phase transition between the exotic inhomogeneous LO phase and the BCS phase. In comparison to the three-dimensional case, where the phase diagram is dominated by a generic separation phase, we predict a broader parameter space for the spatially inhomogeneous LO phase. By computing the superfluid density of the LO phase at different polarization, we show how the superfluidity of the system is suppressed with increasing spin polarization.

I. INTRODUCTION

Superfluidity in fermionic systems has been experimentally and theoretically explored since the seminal experiments performed with ^{3}He in the early 1970s [1,2]. Here it was found that the critical temperature was roughly a thousand times less than the bosonic ^{4}He superfluid transition temperature. The statistical properties of the fermionic system led theorists to consider an analog of the successful Cooper pairs *Ansatz* used in the Bardeen-Cooper-Schrieffer (BCS) theory, describing the superfluid state by a superconducting theory involving particles without electric charge [3]. Although successful in describing the low-temperature behavior of the ^{3}He system, the BCS theory was an incomplete treatment for more complicated systems, such as the case of imbalanced Fermi mixtures. A finite polarization, due to Pauli paramagnetism, is strongly opposed to the BCS-predicted ground state.

The first theoretical attempt to explore polarized fermionic systems was independently performed by Fulde and Ferrell (FF) [4] and by Larkin and Ovchinnikov (LO) [5] and the resulting phase has since then been referred to as the FFLO phase. Starting from the Cooper solution of a fermionic pair that experiences an attractive potential over a Fermi surface, they considered the case where the pair could carry a finite center-of-mass momentum. This situation in the balanced case is energetically costly. It was pointed out by Cooper that pairs with finite center-of-mass momentum are energetically unfavorable due to the increase of internal energy from the pair-drift velocity [6]. In the case of an imbalanced system, where the Fermi surfaces of different components do not fully overlap, however, the most favorable energetic configuration of the ground state has a spatially inhomogeneous order parameter, compared with the BCS solution of a uniform order parameter. In an imbalanced system, Fulde and Ferrel proposed an *Ansatz* for the order parameter of the form

$\Delta(\mathbf{x}) = \Delta_0 \exp(i\mathbf{Q} \cdot \mathbf{x})$, where Δ_0 is a constant parameter and $\mathbf{Q}$ plays the role of the nonvanishing pair center-of-mass momentum [4]. Larkin and Ovchinnikov proposed the sum of two opposite plane waves with the same momentum, $\Delta(\mathbf{x}) = \Delta_0 \cos(\mathbf{Q} \cdot \mathbf{x})$ [5].

Understanding these exotic inhomogeneous superfluid phases has attracted considerable experimental and theoretical attention over the past fifty years in different branches of physics. The study of the FFLO phase has been of great interest to the condensed-matter community, where the FFLO could be a candidate phase in heavy-fermion superconductors such as CeCoIn$_5$ at large in-plane Zeeman fields [7–9]. The observation of anisotropic conductivity in organic superconducting compounds indicates that these materials may represent an interesting system to accommodate this inhomogeneous order-parameter phase [10,11]. The FFLO state is of interest in quantum chromodynamics where it may be favored at low temperature and high density [12]. However, so far, conclusive signatures of a spatially inhomogeneous superfluid phase have yet to be clearly demonstrated.

Over the past decade, ultracold Fermi gases have offered a unique environment to explore population-imbalanced fermionic systems [13–16]. The controllability of ultracold experiments allows the tuning of interactions between fermions through Feshbach resonances to access a broad range of different interaction regimes [17,18]. The combination of available techniques, such as optical lattices [19,20], radio-frequency-driven (spin) population imbalance [21], and exotic interactions such as spin-orbit coupling [22,23], has opened up new methods to probe the existence of any novel phases that are strongly believed to occur at low temperatures. However, the existence of the FFLO phase in cold-atom systems is yet to be confirmed. The lack of experimental observation of the FFLO phase in three dimensions can be understood from the fragile nature and small region of the phase space where the FFLO is energetically favorable [24–26].

There are alternative scenarios to explain pairing in the presence of imbalance, like breached pairing [27] and Sarma
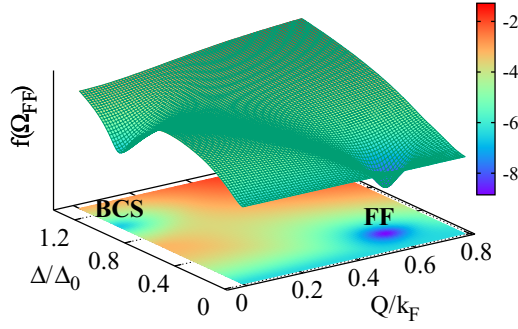
_____
[*]utoniolo@swin.edu.au

FIG. 1. Thermodynamic potential per particle for the FF *Ansatz* in two dimensions. The z axis is rescaled by using a logarithmic function $f(z) = \ln(1 + \alpha z/(2\pi\varepsilon_F))$, with $\alpha = 9.916$.

states [28–30], which directly compete against the FF *Ansatz* being a local maximum of the FF thermodynamic potential in Fig. 1. Both of these cases suffer, in three-dimensions (3D), from the instability towards a phase-separation phase [31], in which the BCS superfluid coexists with a normal fraction; thus they will not be considered in this work.

A promising method to study imbalanced Fermi gases and the FFLO phase is through evolving the system in reduced dimensions. Anisotropy-related effects such as exotic inhomogeneous superfluid phases can be enhanced and stabilized by Fermi surface "nesting" in low-dimensional systems [32–34]. A full one-dimensional (1D) configuration [35] and a suitable experimental setup has been investigated [36], providing new interesting hints for the FFLO-phase observation and detection. In two-dimensional (2D) systems the problem has been theoretically analyzed by testing the FF *Ansatz* [37,38] or LO *Ansatz* with linearized single-particle dispersion relation [39], by considering square lattices within both FF and LO theories [40], and by investigating beyond-mean-field effects with an FF order parameter [41]. It is worth noting that, recently, there has been rapid progress in experimentally probing 2D Fermi gases [42–45]. We anticipate that these advancements will be of great importance in finding the FFLO phase.

Theoretical results suggest that the FF *Ansatz* is not the most energetically favorable choice and that the LO *Ansatz* describes the preferred ground state [16]. In this work, we build upon this idea and extensively explore the LO-type *Ansatz* in 2D imbalanced Fermi gases through the Bogoliubov-de Gennes (BdG) mean-field theory and determine the phase space where the LO-type phase is energetically favorable.

This work is structured as follows: In Sec. II we describe the FFLO family and set the appropriate notations of the *Ansatz* of the order parameter to be used in this paper. The model is described in Sec. III, including the relevant scattering theory, BdG formulation, and computational implementation of the model. Section IV is devoted to the results where we discuss the canonical ensemble first and then the grand canonical ensemble. Section V contains the results of the superfluid density of the LO phase. Finally, in Sec. VI we present our conclusions.

II. THE FULDE-FERRELL-LARKIN-OVCHINNIKOV FAMILY

For the sake of clarification we provide a summary of the definitions of the main cases in the FFLO family. The most

generic order parameter for an imbalanced Fermi gas in a box with sides L and volume $V = L^\nu$, for arbitrary dimension $\nu > 1$ that satisfies periodic boundary conditions is a Fourier transform over the discretized modes of the box,

$$\Delta_{\text{FFLO}}(\mathbf{x}) = \sum_{\mathbf{Q}} \Delta_{\mathbf{Q}} \exp(i\mathbf{Q} \cdot \mathbf{x}), \tag{1}$$

with $\mathbf{Q} \in \mathbb{Z}^\nu$. Within this family many further approximations and simplifications may be made; for example, we can choose a single vector $\mathbf{Q}$ and obtain the FF *Ansatz* for the order parameter,

$$\Delta_{\text{FF}}(\mathbf{x}) = \Delta_{\mathbf{Q}} \exp(i\mathbf{Q} \cdot \mathbf{x}). \tag{2}$$

We show in Fig. 1 the thermodynamic potential per particle for the FF *Ansatz* in 2D for chemical potential, $\mu = \varepsilon_F$, chemical-potential difference, $\delta\mu = 0.65\varepsilon_F$, and interaction strength, $\varepsilon_B = 0.35\varepsilon_F$, as a function of the pair momentum $Q = |\mathbf{Q}|$. The order parameter is rescaled with the 2D BCS order parameter, $\Delta_0 = \sqrt{\varepsilon_B(\varepsilon_B + 2\mu)}$ in the balanced limit. The appearance of the FF minimum in Fig. 1, at $Q \sim k_F$, indicates a first-order phase transition from the BCS minimum. The transition from FF to the partially polarized normal state is second order, at which the FF minimum merges with the free Fermi gas line ($\Delta = 0$). These results are found in the thermodynamic limit where the saddle-point approximation of the thermodynamic potential can be analytically written by integrating the fermionic path integrals after a Hubbard–Stratonovich transformation. This case has been extensively studied and used to understand the generic features of the FFLO phase in 2D [37,38]. The FF *Ansatz*, however, is not the most energetically favorable ground state. It has been shown that, for general dimensions, a sum over $\mathbf{Q}$ momenta is favorable [46,47].

If we consider the summation in Eq. (1) of momenta $\mathbf{Q}$ and $-\mathbf{Q}$, we find a standing wave, the LO *Ansatz*,

$$\Delta_{\text{LO}}(\mathbf{x}) = \Delta_{\mathbf{Q}} \cos(\mathbf{Q} \cdot \mathbf{x}). \tag{3}$$

The LO *Ansatz* suffers from the loss of an analytic formula for the thermodynamic potential as the fermionic fields cannot be integrated out analytically from the partition function. To this end, some efforts to obtain a truncated approximation of the thermodynamic potential in 3D have provided interesting qualitative results [48].

The LO *Ansatz* in Eq. (3) can be further simplified by requiring the order parameter to depend on a single direction. It has been shown in 2D and 3D that the spontaneous breaking of symmetry due to the LO transition essentially occurs in a random direction only, and in 3D it occurs in a very narrow region of the phase diagram [16]. The cost of the diagonalization of the Hamiltonian can be reduced in complexity and a complete study becomes tractable. Specifically, we have for a given momentum $\mathbf{Q}$ along the x axis the pairing order parameter

$$\Delta_{\text{LO}_1}(\mathbf{x}) = \Delta_Q \cos(Qx), \tag{4}$$

and we refer to this as the LO_1 pairing order parameter. This approach allows us to model the order parameter as a much more detailed function as long as we keep the phase-transition symmetry breaking in one direction. In particular, we are able to study a generalization of the LO_1 phase that will be called

LO_g through the whole work,

$$\Delta_{LO_g}(\mathbf{x}) = \sum_Q \Delta_Q \cos(Qx), \tag{5}$$

where Q here is summed over the box modes in a single direction under a periodic boundary condition. This choice includes the largest number of Q choices available in a finite box and turned out to be, in 1D, energetically favorable with respect to the single Q choice in the FF *Ansatz* and the double Q choice of the LO_1 [35]. If we exclude the dependency of the order parameter on more than a single direction in space, the LO_g represents again the most general *Ansatz*.

For the sake of completeness, we mention that the multidirectional symmetry-breaking phase transition is referred to as LO_2. When the system experiences a large population imbalance, the order parameter may depend on two or three directions in space. It can be argued that, for symmetry reasons, similar to the LO phase discussion, the LO_2 transition should occur with $Q_i = Q$ in any ith direction, leading to a form $\Delta_{LO_2}(\mathbf{x}) = \Delta_Q[\cos(Qx) + \cos(Qy)]$ in two and three dimensions, or $\Delta_{LO_3}(\mathbf{x}) = \Delta_Q[\cos(Qx) + \cos(Qy) + \cos(Qz)]$ in three dimensions. The role played by these phases involves only a small part of the phase diagram at large polarization [48], and we can neglect them from the main study of the LO_g phase.

III. MODEL

In this work we consider a polarized Fermi gas in the 2D regime through a single-channel model. Highly oblate systems can be realized via a combination of harmonic traps along the radial and axial directions, where the anisotropic aspect ratio is $\lambda = \omega_z/\omega_\rho$, for axial confinement, ω_z, and the radial counterpart denoted by ω_ρ. When the temperature of the gas, $k_B T$, is significantly smaller than the energy spacing of the harmonic-oscillator states, $\hbar\omega_z$ or $\hbar\omega_\rho$, the condition $k_B T \ll \hbar\omega_z \ll \hbar\omega_\rho/N$ describes a 1D regime with the transverse direction frozen, while the condition

$$k_B T \ll \hbar\omega_\rho \ll \hbar\omega_z/\sqrt{N} \tag{6}$$

freezes out the axial direction and describes a 2D system. The 2D Fermi gas is then described by the following effective single-channel Hamiltonian:

$$\mathcal{H} = \sum_\sigma \left[\int_V d^2x \, \psi_\sigma^*(\mathbf{x})\left(-\frac{\hbar^2}{2m}\nabla^2 - \mu_\sigma \right)\psi_\sigma(\mathbf{x}) \right]$$
$$+ g_{2D} \int_V d^2x \, \psi_\uparrow^*(\mathbf{x})\psi_\downarrow^*(\mathbf{x})\psi_\downarrow(\mathbf{x})\psi_\uparrow(\mathbf{x}), \tag{7}$$

where $\psi_\sigma(\mathbf{x})$ is the Fermi field operator with pseudospins $\sigma = \uparrow, \downarrow$, V is the area of the system, g_{2D} is the magnitude of the contact interaction, $\mu_\uparrow = \mu + \delta\mu$ and $\mu_\downarrow = \mu - \delta\mu$ are the chemical potentials for the spin components, $\delta\mu$ is the chemical potential imbalance, and m is the mass of the atoms. We define the polarization of the system in terms of the populations $N_\uparrow$ and $N_\downarrow$,

$$p = \frac{N_\uparrow - N_\downarrow}{N_\uparrow + N_\downarrow}, \tag{8}$$

where $N = N_\uparrow + N_\downarrow$ is the total number of atoms in the system. The interaction is modeled as a contact potential

in the s-wave channel, $U_{2D}(\mathbf{x},\mathbf{x}') = g_{2D}\delta(\mathbf{x} - \mathbf{x}')$, and in two dimensions must be carefully dealt with. The contact interaction should be renormalized due to the unphysical ultraviolet divergence (UV) at high energy. From the two-body T matrix we have

$$T^{-1}(E) = V g_{2D}^{-1} - \Pi(E), \tag{9}$$

where E is the scattering energy in the center-of-mass frame, the particle-particle bubble is given by

$$\Pi(E) = \sum_{\mathbf{k}} \frac{1}{E - 2\varepsilon_{\mathbf{k}} + i0^+}, \tag{10}$$

and $\varepsilon_{\mathbf{k}} = \hbar^2\mathbf{k}^2/2m$. The particle-particle bubble diverges logarithmically in two dimensions and we regularize this by introducing a cutoff Λ for large k. We match the s-wave 2D scattering amplitude to the two-body T matrix,

$$T(E) = \frac{4\pi\hbar^2/m}{\ln(\varepsilon_B/E) + i\pi}, \tag{11}$$

in the zero-energy limit and for the binding energy ε_B of the two-body bound state. The scattering amplitude can be recovered from the contact potential by setting and defining,

$$\frac{1}{g_{2D}(\Lambda)} = -\frac{1}{V}\sum_{|\mathbf{k}|<\Lambda} \frac{1}{2\varepsilon_{\mathbf{k}} + \varepsilon_B}. \tag{12}$$

The two-body binding energy is then related to the 2D scattering length via

$$\varepsilon_B = \frac{\hbar^2}{ma_{2D}^2}. \tag{13}$$

It is useful to compare 2D scattering to its 3D counterpart, describing how a quasi-2D system is related to a 3D system [49,50]. Integrating out the axial direction we can relate the 3D scattering length to an effective quasi-2D scattering length,

$$\frac{a_{2D}}{l_z} = \sqrt{\frac{\pi}{B}}\exp\left(-\sqrt{\frac{\pi}{2}}\frac{l_z}{a_{3D}} \right), \tag{14}$$

where $l_z = \sqrt{\hbar/(m\omega_z)}$ is the axial harmonic-oscillator length and $B \simeq 0.905$ is a constant. Equation (14) is valid when the scattering energy is negligible compared with the strength of the confinement. In actual experiments, the scattering length, a_{2D}, can be changed via Feshbach resonances and hence the effective interactions can be tuned [45].

A. Bogoliubov–de Gennes self-consistent method

We now turn to the many-body formulation of a population-imbalanced Fermi gas considered through the BdG equations. Starting from the Heisenberg equation of motion of the Hamiltonian found in Eq. (7), we define $\mathrm{sgn}(\uparrow) = -\mathrm{sgn}(\downarrow) = 1$ and we obtain for the fermionic fields $\psi_\sigma(\mathbf{x},t)$,

$$i\partial_t\psi_\sigma = \left(-\frac{\hbar^2\nabla^2}{2m} - \mu_\sigma \right)\psi_\sigma + g_{2D}(\mathrm{sgn}\,\sigma)\psi_{\bar\sigma}^*\psi_\downarrow\psi_\uparrow. \tag{15}$$

Via the mean-field approximation, we can replace the coupled terms, $g_{2D}\psi_\uparrow^\dagger\psi_\downarrow\psi_\uparrow$ and $g_{2D}\psi_\uparrow^\dagger\psi_\downarrow\psi_\uparrow$ with their respective

mean fields,

$$g_{2D}(\text{sgn}\,\sigma)\psi_{\bar{\sigma}}^*\psi_\downarrow\psi_\uparrow \simeq g_{2D}n_{\bar{\sigma}}(\mathbf{x})\psi_\sigma - (\text{sgn}\,\sigma)\Delta(\mathbf{x})\psi_{\bar{\sigma}}^*, \quad (16)$$

where we have defined the order parameter and the density profiles, $\Delta(\mathbf{x}) = -g_{2D}\langle\psi_\downarrow(\mathbf{x})\psi_\uparrow(\mathbf{x})\rangle$ and $n_\sigma(\mathbf{x}) = \langle\psi_\sigma^\dagger(\mathbf{x})\psi_\sigma(\mathbf{x})\rangle$. The above decoupling of the fields gives the following to the equations of motion for the spin component σ:

$$i\frac{\partial\psi_\sigma}{\partial t}(\mathbf{x},t) = (\mathcal{H}_0 - \mu_\sigma)\psi_\sigma(\mathbf{x},t) - \text{sgn}(\sigma)\Delta(\mathbf{x})\psi_{\bar{\sigma}}^\dagger(\mathbf{x},t),$$
$$(17)$$

where $\mathcal{H}_0 = -\hbar^2\nabla_\mathbf{x}^2/(2m)$. Note that we will discard the Hartree term as we take $g_{2D} \to 0$ in the renormalization procedure. We insert the standard Bogoliubov transformation to solve the equations of motion,

$$\psi_\uparrow(\mathbf{x},t) = \sum_\eta [u_{\eta\uparrow}(\mathbf{x})c_{\eta\uparrow}e^{-iE_{\eta\uparrow}t} - v_{\eta\downarrow}^*(\mathbf{x})c_{\eta\downarrow}^\dagger e^{iE_{\eta\downarrow}t}],$$

$$\psi_\downarrow^\dagger(\mathbf{x},t) = \sum_\eta [u_{\eta\downarrow}^*(\mathbf{x})c_{\eta\downarrow}^\dagger e^{iE_{\eta\downarrow}t} + v_{\eta\uparrow}(\mathbf{x})c_{\eta\uparrow}e^{-iE_{\eta\uparrow}t}],$$

where the wave functions $u_{\sigma\eta}(\mathbf{x})$ and $v_{\sigma\eta}(\mathbf{x})$ are normalized by the condition

$$\int_V d\mathbf{x}(|u_{\sigma\eta}(\mathbf{x})|^2 + |v_{\sigma\eta}(\mathbf{x})|^2) = 1. \quad (18)$$

This gives the well-known BdG equations,

$$\begin{bmatrix} \mathcal{H}_0 - \mu_\sigma & -\Delta(\mathbf{x}) \\ -\Delta^*(\mathbf{x}) & -\mathcal{H}_0 + \mu_{\bar{\sigma}} \end{bmatrix}\begin{bmatrix} u_{\eta\sigma}(\mathbf{x}) \\ v_{\eta\sigma}(\mathbf{x}) \end{bmatrix} = E_{\eta\sigma}\begin{bmatrix} u_{\eta\sigma}(\mathbf{x}) \\ v_{\eta\sigma}(\mathbf{x}) \end{bmatrix}, \quad (19)$$

for quasiparticle energy $E_{\eta\sigma}$. The unequal spin populations require the chemical potential of each spin component to be unequal; this leads to different quasiparticle wave functions for each spin component; however, the $\downarrow$ problem is related to the $\uparrow$ problem through the unitary transformation

$$\begin{bmatrix} u_{\eta\sigma}(\mathbf{x}) \\ v_{\eta\sigma}(\mathbf{x}) \end{bmatrix} = \begin{bmatrix} -v_{\eta\bar{\sigma}}^*(\mathbf{x}) \\ u_{\eta\bar{\sigma}}^*(\mathbf{x}) \end{bmatrix}, \quad (20)$$

and the real-valued quasiparticle energies through $E_{\eta\sigma} = -E_{\eta\bar{\sigma}}$. Without loss of generality we then remove the spin index of the BdG equations, defining $u_\eta = u_{\eta\uparrow}$, $v_\eta = v_{\eta\uparrow}$, and $E_\eta = E_{\eta\uparrow}$, leading to the following form:

$$\begin{bmatrix} \mathcal{H}_0 - \mu_\uparrow & -\Delta(\mathbf{x}) \\ -\Delta^*(\mathbf{x}) & -\mathcal{H}_0 + \mu_\downarrow \end{bmatrix}\begin{bmatrix} u_\eta(\mathbf{x}) \\ v_\eta(\mathbf{x}) \end{bmatrix} = E_\eta\begin{bmatrix} u_\eta(\mathbf{x}) \\ v_\eta(\mathbf{x}) \end{bmatrix}. \quad (21)$$

Through the Bogoliubov transforms the density profiles $n_\sigma(\mathbf{x})$ can be written in terms of the quasiparticle creation and annihilation operators,

$$n_\uparrow(\mathbf{x}) = \sum_\eta u_\eta^*(\mathbf{x})u_\eta(\mathbf{x})f(E_\eta), \quad (22)$$

$$n_\downarrow(\mathbf{x}) = \sum_\eta v_\eta^*(\mathbf{x})v_\eta(\mathbf{x})f(-E_\eta), \quad (23)$$

and the pairing gap function becomes

$$\Delta(\mathbf{x}) = -g_{2D}\sum_\eta u_\eta(\mathbf{x})v_\eta^*(\mathbf{x})f(E_\eta). \quad (24)$$

The contact interaction introduces a UV divergence in the order parameter and this will be dealt with in the next

section. We impose fermionic statistics for excitations at inverse temperature $\beta = 1/(k_B T)$ through the Fermi-Dirac distribution $f(E_\eta) = 1/(1 + e^{\beta E_\eta})$.

B. Bogoliubov-de Gennes equations with the LO$_g$ *Ansatz*

The first step to solve the BdG equations is to expand the quasiparticle wave functions onto a complete basis and define the order parameter as being a real-valued function. The complete basis we will use is a tensor product of a 1D complete orthonormal basis that satisfies the periodic boundary conditions of a box with length L. Specifically, for a given $\mathbf{n} = (n_1, n_2) \in \mathbb{N} \times \mathbb{N}$, we have

$$\phi_\mathbf{n}^{(2)}(\mathbf{x}) = \phi_{n_1}^{(1)}(x) \otimes \phi_{n_2}^{(1)}(y), \quad (25)$$

where

$$\phi_n^{(1)}(x) = \begin{cases} L^{-1/2} & \text{if } n = 0 \\ (2/L)^{1/2}\cos[n\pi x/L] & \text{if } n \text{ is even} \\ (2/L)^{1/2}\sin[(n+1)\pi x/L] & \text{if } n \text{ is odd}, \end{cases} \quad (26)$$

and n_1 and n_2 are non-negative integers. Letting $\hbar = 2m = 1$, the 1D basis functions, $\phi_n^{(1)}(x)$, are eigenvectors for the one-dimensional free Hamiltonian, $\mathcal{H} = -(d^2/dx^2)$, with eigenvalues

$$\varepsilon_n := \begin{cases} \pi^2 n^2/L^2 & \text{if } n \text{ is even} \\ \pi^2(n+1)^2/L^2 & \text{if } n \text{ is odd}. \end{cases} \quad (27)$$

The product basis, Eq. (25), are eigenvectors for $\mathcal{H}_0$ with eigenvalues $\varepsilon_\mathbf{n} = \varepsilon_{n_1} + \varepsilon_{n_2}$. We expand the basis functions $u_\eta(\mathbf{x})$ and $v_\eta(\mathbf{x})$ onto this basis,

$$u_\eta(\mathbf{x}) = \sum_\mathbf{n} A_\mathbf{n}^{(\eta)}\phi_\mathbf{n}^{(2)}(\mathbf{x}), \quad v_\eta(\mathbf{x}) = \sum_\mathbf{m} B_\mathbf{m}^{(\eta)}\phi_\mathbf{m}^{(2)}(\mathbf{x}),$$

and the BdG equations (21) become

$$\begin{bmatrix} (\varepsilon_\mathbf{n} - \mu_\uparrow)\delta_{\mathbf{nm}} & -\Delta_{\mathbf{nm}} \\ -\Delta_{\mathbf{nm}}^* & -(\varepsilon_\mathbf{n} - \mu_\downarrow)\delta_{\mathbf{nm}} \end{bmatrix}\begin{bmatrix} A_\mathbf{m}^{(\eta)} \\ B_\mathbf{m}^{(\eta)} \end{bmatrix} = E_\eta\begin{bmatrix} A_\mathbf{n}^{(\eta)} \\ B_\mathbf{n}^{(\eta)} \end{bmatrix}, \quad (28)$$

where

$$\Delta_{\mathbf{nm}} = \int_V d^2x\,\phi_\mathbf{n}^{(2)}(\mathbf{x})\Delta(\mathbf{x})\phi_\mathbf{m}^{(2)}(\mathbf{x}). \quad (29)$$

The eigenvalue problem described by Eq. (28) comes at significant computational cost and is not easily tractable. In this work we solve the simpler case of an order parameter $\Delta(\mathbf{x})$ that is a real-valued function depending on the x direction only and is a sum of Q modes, the LO$_g$ *Ansatz* defined in Eq. (5). The periodic boundary conditions force the Fourier transform of $\Delta(\mathbf{x})$ to be dependent on the discretized, even modes of the box. This fixes $Q = 2\pi n/L$ for each non-negative integer $n \in \mathbb{N}$. From Eq. (29), we integrate for each $\mathbf{n} = (n_1, n_2)$ and each $\mathbf{m} = (m_1, m_2)$ over the variable y, i.e.,

$$\Delta_{\mathbf{nm}} = \delta_{n_2,m_2}\int_{-L/2}^{L/2}dx\,\phi_{n_1}^{(1)}(x)\Delta(x)\phi_{m_1}^{(1)}(x),$$
$$= \delta_{n_2,m_2}\Delta_{n_1,m_1}. \quad (30)$$

We can simplify the BdG equations further by exploiting the y dependence of the densities and order parameter for all η in Eqs. (22)–(24), and the BdG equations (28). We see that the dependence on m_2 falls out of the problem and the BdG

equations become block diagonal in n_2. This simplifies the BdG equations and we have for our final form,

$$\begin{bmatrix} \varepsilon_\uparrow & -\Delta_{n_1 m_1} \\ -\Delta_{n_1 m_1} & -\varepsilon_\downarrow \end{bmatrix} \begin{bmatrix} A_{m_1}^{(\eta n_2)} \\ B_{m_1}^{(\eta n_2)} \end{bmatrix} = E_\eta^{n_2} \begin{bmatrix} A_{n_1}^{(\eta n_2)} \\ B_{n_1}^{(\eta n_2)} \end{bmatrix}, \quad (31)$$

where $\varepsilon_\uparrow = (\varepsilon_{n_1 m_1, n_2} - \mu_\uparrow)\delta_{n_1 m_1}$ and $\varepsilon_\downarrow = (\varepsilon_{n_1 m_1, n_2} - \mu_\downarrow)\delta_{n_1 m_1}$.

C. Hybrid Bogoliubov-de Gennes strategy

To deal with the infinite-dimensional size of the BdG equations matrix we introduce a cutoff energy E_c to make the matrix equations finite and treat the high-lying energy states in Eqs. (31) separately as free states or plane-wave functions [35]. Specifically, we have the discrete part, below the cutoff, and a continuous part above the cutoff. From Eqs. (22)–(24) we truncate the sums to obtain

$$n_{d\uparrow}(\mathbf{x}) = \sum_{|E_\eta| < E_c} u_\eta^*(\mathbf{x}) u_\eta(\mathbf{x}) f(E_\eta), \quad (32)$$

$$n_{d\downarrow}(\mathbf{x}) = \sum_{|E_\eta| < E_c} v_\eta^*(\mathbf{x}) v_\eta(\mathbf{x}) f(-E_\eta), \quad (33)$$

$$\Delta_d(\mathbf{x}) = -g_{2D} \sum_{|E_\eta| < E_c} u_\eta(\mathbf{x}) v_\eta^*(\mathbf{x}) f(E_\eta), \quad (34)$$

and where the gap equation is still yet to be renormalized. The high-lying states, treated as plane waves,

$$u_\eta(\mathbf{x}) \to \frac{1}{\sqrt{V}} u_k(\mathbf{x}) e^{i\mathbf{k}\cdot\mathbf{x}},$$

$$v_\eta(\mathbf{x}) \to \frac{1}{\sqrt{V}} v_k(\mathbf{x}) e^{i\mathbf{k}\cdot\mathbf{x}}, \quad (35)$$

allow us to solve Eq. (31) and compute the energies above the cutoff. In particular, we can define the energies $E_k(\mathbf{x}) = [(\varepsilon_k - \mu)^2 + \Delta(\mathbf{x})^2]^{1/2}$ and obtain the continuum corrections,

$$n_{c\uparrow}(\mathbf{x}) = \sum_{\mathbf{k}} \left(\frac{1}{2} - \frac{\varepsilon_k - \mu}{2E_k(\mathbf{x})} \right) \Theta(E_k(\mathbf{x}) + \delta\mu - E_c), \quad (36)$$

$$n_{c\downarrow}(\mathbf{x}) = \sum_{\mathbf{k}} \left(\frac{1}{2} - \frac{\varepsilon_k - \mu}{2E_k(\mathbf{x})} \right) \Theta(E_k(\mathbf{x}) - \delta\mu - E_c), \quad (37)$$

$$\Delta_c(\mathbf{x}) = -g_{2D} \sum_{\mathbf{k}} \frac{\Delta(\mathbf{x})}{2E_k(\mathbf{x})} \Theta(E_k(\mathbf{x}) + \delta\mu - E_c), \quad (38)$$

where $\Theta(x)$ is the Heaviside step function. The continuous and discrete parts of the order parameter can be combined and using the regularization condition we have,

$$\Delta(\mathbf{x}) = -g_{2D}^{\text{eff}}(\mathbf{x}) \sum_{|E_\eta| < E_c} u_\eta(\mathbf{x}) v_\eta^*(\mathbf{x}) f(E_\eta), \quad (39)$$

where

$$\frac{1}{g_{2D}^{\text{eff}}(\mathbf{x})} = \frac{1}{g_{2D}} + g(\mathbf{x}), \quad (40)$$

and using the definition

$$g(\mathbf{x}) = \frac{1}{V} \sum_{\mathbf{k}} \frac{1}{2E_k(\mathbf{x})} \Theta(E_k(\mathbf{x}) + \delta\mu - E_c). \quad (41)$$

In the thermodynamic limit, due to the high density of states beyond the cutoff, the continuous contribution can be analytically solved, giving

$$n_{c\uparrow}(\mathbf{x}) = \frac{1}{8\pi}[E_c - \delta\mu + \mu - k_c(\mathbf{x})^2], \quad (42)$$

$$n_{c\downarrow}(\mathbf{x}) = \frac{1}{8\pi}[E_c + \delta\mu + \mu - k_c(\mathbf{x})^2], \quad (43)$$

$$\frac{1}{g_{2D}^{\text{eff}}(\mathbf{x})} = -\frac{1}{8\pi} \ln\left(\frac{E_c - \delta\mu - \mu + k_c(\mathbf{x})^2}{\varepsilon_B} \right), \quad (44)$$

where we introduce the cutoff momentum, $k_c(\mathbf{x}) = \{\mu + [(E_c - \delta\mu)^2 - \Delta(\mathbf{x})^2]^{1/2}\}^{1/2}$. Gathering together all these results we achieve the final form for the densities profiles,

$$n_\uparrow(\mathbf{x}) = n_{d\uparrow}(\mathbf{x}) + n_{c\uparrow}(\mathbf{x}),$$

$$n_\downarrow(\mathbf{x}) = n_{d\downarrow}(\mathbf{x}) + n_{c\downarrow}(\mathbf{x}), \quad (45)$$

$$\Delta(\mathbf{x}) = -g_{2D}^{\text{eff}}(\mathbf{x}) \Delta_d(\mathbf{x}).$$

In the grand canonical ensemble we find the absolute minimum of the thermodynamic potential, $\Omega = \Omega(\mu, \delta\mu, T) = U - TS - \mu N - \delta\mu\delta N$, where U is the internal energy and S is the entropy. Simulations performed in the canonical ensemble requires more computational effort, where the BdG equations depend self-consistently on μ and $\delta\mu$ that are computed by using the number equations

$$N = -\frac{\partial\Omega}{\partial\mu}, \quad \delta N = -\frac{\partial\Omega}{\partial(\delta\mu)}, \quad (46)$$

converging to a given $\mu(n, \delta n, T)$ and $\delta\mu(n, \delta n, T)$. To find the ground state for momenta Q we minimize the Helmholtz free energy, $F = F(n, p, T) = U - TS$ with respect to Q.

D. Energy and entropy

In addition to the calculation of the order parameter and densities, the complete study of this system, either at zero or finite temperature, requires the total energy and entropy densities. Through the Bogoliubov transformations we define the profiles for the energy density, $E(\mathbf{x})$, and the entropy density, $S(\mathbf{x})$, on quasiparticles modes as

$$E(\mathbf{x}) = \mu_\uparrow n_\uparrow(\mathbf{x}) + \mu_\downarrow n_\downarrow(\mathbf{x}) - \frac{|\Delta(\mathbf{x})|^2}{g} + \sum_\eta \{[|u_\eta(\mathbf{x})|^2$$

$$+ |v_\eta(\mathbf{x})|^2] f(E_\eta) - |v_\eta(\mathbf{x})|^2\}, \quad (47)$$

$$S(\mathbf{x}) = -k_B \sum_\eta \{[f(E_\eta) \ln(f(E_\eta)) + f(-E_\eta) \ln(f(-E_\eta))]\}$$

$$\times [|u_\eta(\mathbf{x})|^2 + |v_\eta(\mathbf{x})|^2]. \quad (48)$$

Since both the energy density and entropy density depend on sums over the eigenvalues, E_η, and eigenvectors, $u_\eta(\mathbf{x})$ and $v_\eta(\mathbf{x})$, we can calculate the energy and entropy densities of the system through the expansion of the discrete and continuous states. It is possible to show that the continuous correction to the entropy density is negligible for high-lying states [51], and we focus on the energy. Treating the high-energy states in the thermodynamic limit, we write $E(\mathbf{x}) = E_d(\mathbf{x}) + E_c(\mathbf{x})$ and get

the following contribution:

$$
E_c(\mathbf{x}) = \frac{1}{8\pi}\left\{\Delta^2\left[\frac{1}{2}\right.\right.
$$

$$
+ \ln\left(\frac{\sqrt{E_- + \sqrt{E_-^2 - \Delta^2}}\sqrt{E_+ + \sqrt{E_+^2 - \Delta^2}}}{\varepsilon_B}\right)\left.\right]
$$

$$
+ \sum_{\sigma=\pm} \frac{E_\sigma}{2}\sqrt{E_\sigma^2 - \Delta^2} - E_c^2 + \delta\mu^2\left.\right\}, \qquad (49)
$$

where for simplicity we define $E_\pm = E_c \pm \delta\mu$.

The solutions to the BdG equations were carried out following an iterative algorithm, self-consistently calculating the order parameter and the density profiles. We perform calculations in either the grand canonical ensemble, fixing μ and $\delta\mu$ and computing the number of particles N and polarization p, or in the canonical ensemble, fixing N and p, and iteratively computing μ and $\delta\mu$. It is important to remark that the nature of the quantities we want to investigate, the Helmholtz free energy and thermodynamic potential, show very small variations while changing the thermodynamic variables. From the knowledge we have from solving the FF *Ansatz* found in Fig. 1, the relative difference needed to see the appearance of new absolute minima in the thermodynamic potential is approximately 10^{-7}. To reach this precision we have to increase both the number of particles, which increases the size of the BdG equations, and the sampling rate over the box length, which increases the integration precision. Once the algorithm reaches convergence, the cutof-energy dependence is tested to ensure the calculations do not depend on the cutoff E_c.

The BdG equations are a mean-field treatment of the imbalanced system and they are expected to be quantitatively incorrect in the strongly correlated regime. However, they will provide constant qualitative results for all interaction strengths and will provide an excellent picture of the system under investigation.

IV. RESULTS

In the calculations we use natural units, such that $\hbar = 2m = k_B = 1$ and, in the case of a nonvanishing polarization, we set $k_F = 1$ where k_F is, at fixed particle number, the free Fermi momentum. In 2D the linear relation between the Fermi energy and the density of particles requires that the size of the box L increases as the square root of the number of particles, N. An increase in the number of particles corresponds to a quadratic increase in the size of the BdG equations. We have used a particle number of $N = 2000$, which corresponds to a box size of $L \simeq 112/k_F$, comparable with similar results in the 1D case [51]. We set the cutoff energy for values $E_c \geqslant 10\varepsilon_F$, where $\varepsilon_F = \hbar^2 k_F^2/2m$ is the Fermi energy; however, some calculations require higher cutoff values. It is interesting to note that, for the self-consistent calculations, a large cutoff E_c

slows down the runtime, but reduces the number of iterations before convergence. The accuracy of the diagonalization process of the BdG equations has been implemented with an additional number $\bar{n}$ of orthonormal basis elements beyond the cutoff energy such that

$$
n_1 < \sqrt{\frac{E_c L^2}{\pi^2} - n_2^2} = \bar{n}. \qquad (50)
$$

In the following sections we look at the results for the $\mathrm{LO_g}$ phase in the canonical ensemble and follow with the treatment of the grand-canonical-ensemble results. We discuss the phase diagram at zero and finite temperature, and the structure of the $\mathrm{LO_g}$ ground states that depends on the spin imbalance. A specific comparison with the $\mathrm{LO_1}$ *Ansatz* will be treated. The behavior in the grand canonical ensemble will be extensively investigated with emphasis on the order of the phase transition.

A. Canonical ensemble

In Fig. 2 we present the $\mathrm{LO_g}$ phase diagram in the canonical ensemble for polarizations p and for reduced temperature, $T/T_F = 0$, and binding energy $\varepsilon_B = 0.25\varepsilon_F$. For a fixed polarization p we define the free Fermi gas Helmholtz free energy at zero temperature $F_{\text{free}}(T = 0, n, p)$ and we introduce a rescaling constant $F_0 = 2\pi \times 10^{-2}\varepsilon_F N$, with N being the number of particles, such that we can plot the dimensionless quantity,

$$
\delta F/F_0 = \left[F_{\mathrm{LO_g}}(T, n, p) - F_{\text{free}}(T = 0, n, p)\right]/F_0. \qquad (51)
$$

We see that the $\mathrm{LO_g}$ phase is the energetically favorable ground state (with respect to the BCS and FF minima) for polarizations $0.02 \leqslant p \leqslant 0.58$, above $p > 0.58$ the system falls into the free Fermi gas phase [52]. We know that a finite nonzero polarization destroys the BCS phase, and we see a transition at very low polarizations, $p_{c1} = 0.02$. The finite nature of this transition is due to the numerical difficulty in finding the true ground state. We expect that, for finite nonvanishing polarizations below the transition, $p < p_{c1}$, the $\mathrm{LO_g}$ phase is
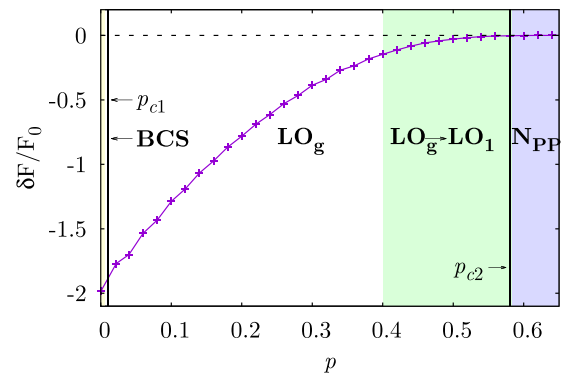

FIG. 2. The energy difference $\delta F = F_{\mathrm{LO_g}} - F_{\text{free}}$, for the Helmholtz free energy, $F_{\mathrm{LO_g}}$, and the free Fermi gas, F_{free}, at temperature $T/T_F = 0$, and interaction strength $\varepsilon_B = 0.25\varepsilon_F$. Rescaled for graphic purposes through the constant $F_0 = 2\pi \times 10^{-2}N\varepsilon_F$. The transition polarization $p_{c1} \simeq 0.02$, from BCS to $\mathrm{LO_g}$, and $p_{c2} = 0.58$, from $\mathrm{LO_g}$ to N_{PP}, are denoted by bold black vertical lines. The region $p > 0.4$ denotes the $\mathrm{LO_g}$ phase that is indistinguishable from the $\mathrm{LO_1}$ phase.
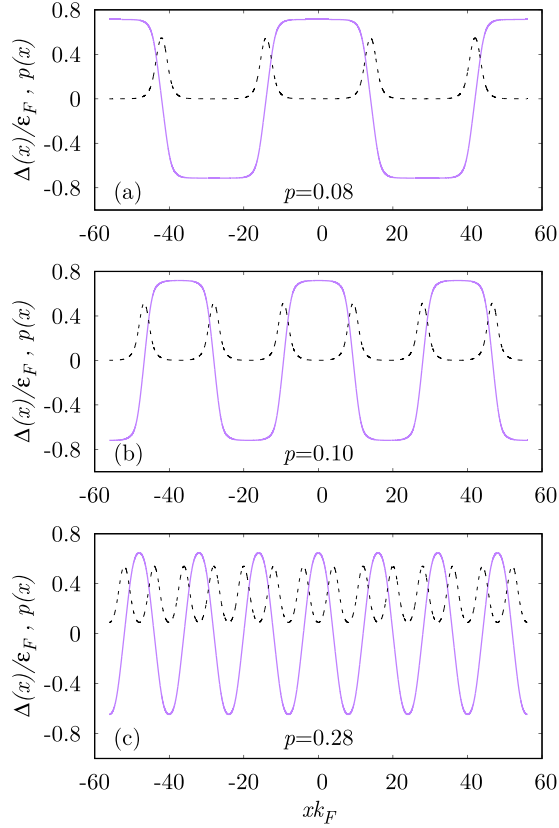
FIG. 3. The inhomogeneous order parameter $\Delta(x)/\varepsilon_F$ as a function of the x direction (solid line) and the local spin polarization $p(x)$ (dashed line) calculated via the self-consistent method at temperature $T/T_F = 0$ and interaction strength $\varepsilon_B = 0.25\varepsilon_F$, for polarizations (a) $p = 0.08$, (b) $p = 0.10$, and (c) $p = 0.28$.
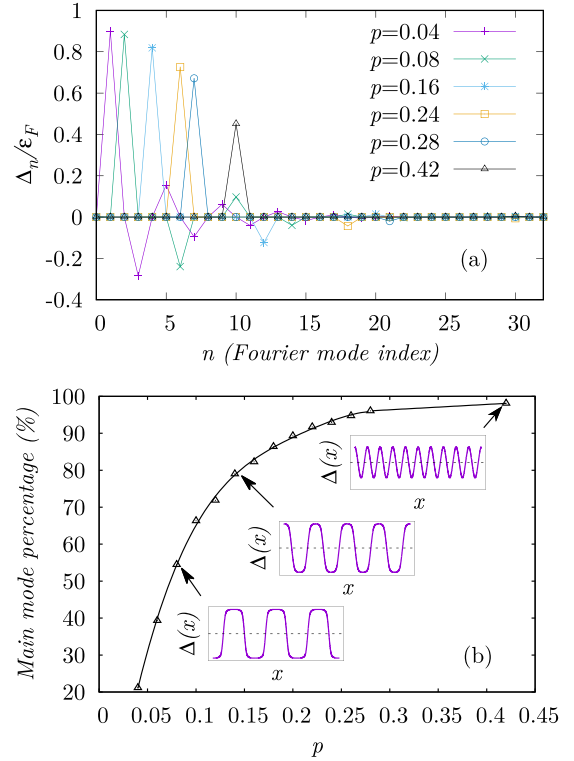

FIG. 4. (a) The weight Δ_n (in Fermi energy units) of each Fourier cosine mode n of the LO_g phase, calculated according to Eq. (53) at zero temperature and $\varepsilon_B = 0.25\varepsilon_F$, at different spin polarizations p. (b) The weight of the main Fourier mode, shown in percentage with respect to the other nonvanishing modes, as a function of the spin polarization. The insets are a guide to show the behavior of the order parameter for a given polarization.

still the ground state. At high polarizations $0.40 < p < 0.58$ the LO_g and LO_1 phase have merged, and we explore and elucidate this part of the phase diagram further below through the structure of the order parameter.

In Fig. 3 we explore the spatial distribution of the order parameter (solid line) and the local spin polarization (dashed line),

$$p(x) = \frac{n_\uparrow(x) - n_\downarrow(x)}{n_\uparrow(x) + n_\downarrow(x)}, \tag{52}$$

from the converged BdG solutions for polarizations $p = 0.08$ [Fig. 3(a)], $p = 0.10$ [Fig. 3(b)], and $p = 0.28$ [Fig. 3(c)] as a function of the box length xk_F, where k_F is the Fermi momentum. We see in Figs. 3(a)–3(c) that the increasing polarization p leads to a higher main amplitude Q and becomes consistent with the LO_1 Ansatz. The local spin polarization is plotted as a function of space and we observe the structure imposed by the LO_g phase. We see the favorable ground-state configuration places the excess spin-up atoms (the majority) where the order parameter vanishes, and the superfluid fraction at the peaks, and here excitations are less probable to occur, preserving superfluidity.

We can compare the LO_g ground-state order parameter with the LO_1 Ansatz, by decomposing the self-consistently computed order parameter through a cosine Fourier transform.

The order parameter has to be an even function along the chosen preferred direction; that is,

$$\Delta_{LO_g}(x) = \sum_{n=1}^{\infty} \Delta_n \cos\left(\frac{2\pi n}{L}x\right), \tag{53}$$

then the LO_g and the LO_1 are the same phase when the Fourier transform has only one mode. In Fig. 4(a) we show that the self-consistent LO_g phase is a superposition of different Fourier cosine modes and has a main mode occupation that is provided by the LO_1 Ansatz. A comparison between the LO_g phase configuration versus the LO_1 indicates that the LO_g choice is always energetically favorable. This fact is true at both low and high polarizations where the LO_g and LO_1 phases almost match. To explore this overlap we study the percent occupation of the main mode and we observe in Fig. 4(b) that a perfect overlap between the phases never fully occurs. We can then conclude that there is always a combination of modes that is the energetically preferred ground state.

In Fig. 5 we show the behavior of the Helmholtz free energy for two different cases: at zero temperature and letting the polarization vary [Fig. 5(a)], while in Fig. 5(b) the polarization is fixed at $p = 0.07$ and we increase the temperature. Figure 5(a) shows that the minimum of the free energy that occurs at $Q_{\min}$ always lies away from $Q/k_F = 0$ and $Q_{\min}$ increases proportionally with the polarization. Figure 5(b) shows that
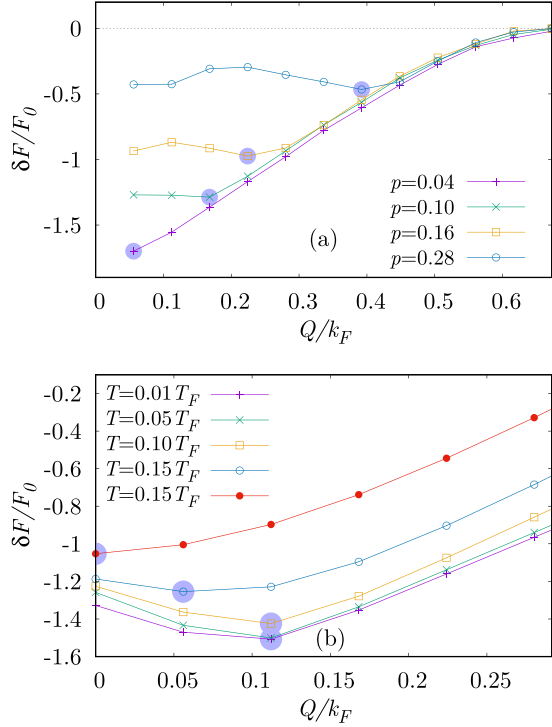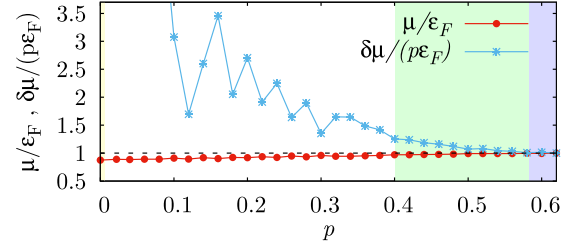
FIG. 6. The behavior of μ and $\delta\mu$ with respect to their expected behavior as free Fermi gas thermodynamic variables, as a function of the polarization, at zero temperature, density $n = k_F^2/(2\pi)$ and binding energy $\varepsilon_B = 0.25\varepsilon_F$. The phase transition in the canonical ensemble are denoted by the background color as found in Fig. 2.

FIG. 5. The Helmholtz free-energy difference between the LO_g (for $Q \neq 0$ and BCS at $Q = 0$) and the free Fermi gas free energy rescaled by $F_0 = 2\pi \times 10^{-2} N\varepsilon_F$: (a) at zero temperature varying the polarization and (b) at fixed polarization $p = 0.07$ increasing the temperature. The semitransparent bullets indicate the absolute minimum position $Q_{\min}$ for each configuration. The dashed horizontal line in panel (a) is the free Fermi gas free energy: every time the Q is too high the model mimics the free Fermi gas destroying the order parameter. Here, the binding energy is $\varepsilon_B = 0.25\varepsilon_F$.

there is a transition point between the LO_g phase and the BCS phase in the temperature range $0.15T_F < T < 0.20T_F$. We observe that the increase of polarization pushes the minimum to high Q values, while the increase of temperature pushes it back towards the $Q = 0$ limit (i.e., the BCS phase). This behavior is expected to change for high polarization when the LO_g phase has a transition directly to the free Fermi gas phase. We note that the interaction strength $\varepsilon_B = 0.25\varepsilon_F$ requires a pair-fluctuation treatment to produce quantitative results as the mean-field theory predicts the transition temperature from the BCS to normal state of $0.41T_F$, well above the experimental observations [42,53].

B. Grand canonical ensemble

Although the canonical ensemble can tell us about the properties and exotic phases of a spin-polarized Fermi gas, it is important to know the nature of the phase transitions and the transition temperatures of the phases we have described so far; to perform this we now work in the grand canonical ensemble. The absolute minimum of the thermodynamic potential is found at fixed chemical potentials μ and $\delta\mu$, and this minimum moves through the landscape of the thermodynamic potential, giving us an insight as to the order of each phase transition. To explore the system we first need to study the behavior

of the chemical potentials μ and $\delta\mu$, found through the self-consistent BdG method in the canonical ensemble. We explore different regimes through the equations of state, $\mu(n,\delta n)$ and $\delta\mu(n,\delta n)$, with respect to a fixed density $n = k_F^2/(2\pi)$ and varying polarization to justify the regimes of interest in the grand canonical ensemble.

The values of μ and $\delta\mu$ used to compute the real order parameter $\Delta(x)$ at fixed density n and polarization p, normalized by the Fermi energy and polarization multiplied by the Fermi energy, respectively, are plotted in Fig. 6. The shaded regions correspond to the phases found in Fig. 2, at polarization $p_{c1} \simeq 0.02$, where we have the transition from BCS to LO_g, and $p_{c2} = 0.58$, for the transition from LO_g to N_{PP} [54]. At zero temperature, the BCS phase is favorable only at $p = 0$. The underlying mean-field theory in 2D for the equation of state of a possible phase-separation phase (i.e., a mixture of a BCS superfluid and a normal gas) has been studied in Ref. [55] and the $\delta\mu$ versus μ phase diagram that involves the transition between BCS phase and the free Fermi gas has been explored therein. We take the salient results here,

$$\mu_{BCS} = \frac{\pi\hbar^2}{m}n - \frac{\varepsilon_B}{2}, \quad 0 \leqslant \delta\mu < \frac{\Delta_0}{\sqrt{2}}. \quad (54)$$

The upper limit for $\delta\mu$ is the Chandrasekhar–Clogston (CC) limit,

$$\delta\mu_{CC} = \sqrt{\frac{\varepsilon_B^2}{2} + \mu\varepsilon_B}, \quad (55)$$

above which the superfluid breaks down. We observe that both μ and $\delta\mu$ assume an almost direct proportionality with the Fermi energy ε_F and the polarization p whenever $\delta\mu$ is large enough. Since in the grand canonical ensemble the LO_g phase arises at high $\delta\mu$, we consider the case of $\mu/\varepsilon_F = 1$ and vary $\delta\mu$ through the CC limit at different binding energies.

Taking the above values for the chemical potentials, in Fig. 7 we plot the phase diagram of the spin-imbalanced Fermi gas as a function of the binding energy, $\varepsilon_B/\varepsilon_F$, and dimensionalized chemical-potential difference, $\delta\mu/\varepsilon_F$. The dashed line represents the CC limit, and we observe that the LO_g phase provides two transition lines that we will denote with $\delta\mu_1$ (stars), below the CC limit, and $\delta\mu_2$ (squares), above it. In particular, the $\delta\mu_2$ line is in agreement with the results provided by the FF *Ansatz* in Ref. [38]. It is interesting to observe how the reduced dimensionality of the problem, at
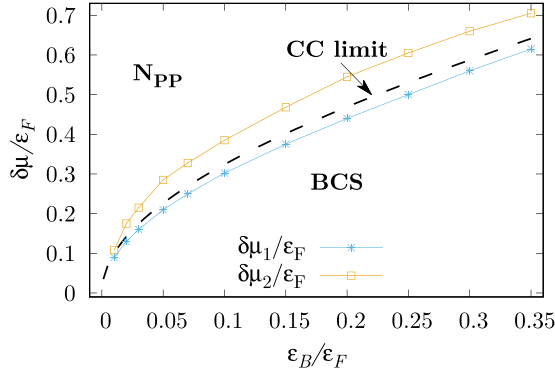
FIG. 7. The critical phase-transition values of $\delta\mu$ as a function of the binding energy ε_B at zero temperature, $\delta\mu_1$ (stars) from the BCS superfluid to LO_g and $\delta\mu_2$ (crosses) from LO_g to N_{PP}.

least at zero temperature, enhances the effect of both the FF and the LO_g phase. In 3D, it is possible to estimate that the FFLO phase is available for roughly 4% of the $\delta\mu$ values for which a superfluid phase is favorable, either BCS or FF, as evaluated from the phase diagram temperature versus magnetization [56]. We find from examining the corresponding region in Fig. 7 that, at a fixed binding energy, the FFLO is accessible for roughly 17% of the phase space, in which the system is a superfluid; that is, $(\delta\mu_2 - \delta\mu_1)/\delta\mu_2 \simeq 0.17$.

We can find the favorability of the LO_g phase compared with the BCS and FF phases by finding the absolute minima of the thermodynamic potential. In Fig. 8 we plot the local minima of the thermodynamic potential of three different *Anätze*: BCS, FF, and LO_g, for two binding energies, $\varepsilon_B = 0.10\varepsilon_F$ [Fig. 8(b)] and $\varepsilon_B = 0.25\varepsilon_F$ [Fig. 8(a)]. Varying the dimensionless chemical-potential difference, $\delta\mu/\Delta_0$, where Δ_0 is the BCS order parameter at zero temperature, we determine the region where the LO_g phase is favorable. The intersection of different phases determines the critical values $\delta\mu_1$ (i.e., from the BCS to LO_g transition) and $\delta\mu_2$ (i.e., from the LO_g to N_{PP} transition).

We see in Fig. 8 that the LO_g to N_{PP} transition is smooth [57] while the BCS to LO_g has a discontinuity, although not easy to observe. The order of the BCS-LO_g transition can be examined as we increase the binding energy ε_B. We check the behavior of the order of phase transitions in Fig. 9, where we have plotted the thermodynamic potential of the LO_g phase as a function of Q at the points labeled (1)–(4) in Fig. 8(a) for the interaction strength $\varepsilon_B = 0.10\varepsilon_F$, sliced at different $\delta\mu$ values. The comparison between subplots in Figs. 9(c) and 9(d) reveals the second-order nature of the LO_g-N_{PP} phase transition. In this part of the phase diagram, an increase of $\delta\mu$ leads to: (i) an increase of the LO momentum Q, (ii) the order-parameter amplitude squeezes until it vanishes in $\delta\mu_2$, and (iii) the order-parameter frequency matches the LO_1 initial *Ansatz*. The BCS-LO_g phase transition can be studied by observing the evolution of the thermodynamic potential in the subplots in Figs. 9(a) and 9(b). It is known that the FF phase undergoes a first-order phase transition towards the BCS phase [38]. In our case, the presence of a local maximum at small Q in the subplot in Fig. 9(a) is an indication of the first-order phase transition. However, within our accuracy, the local maximum is shown
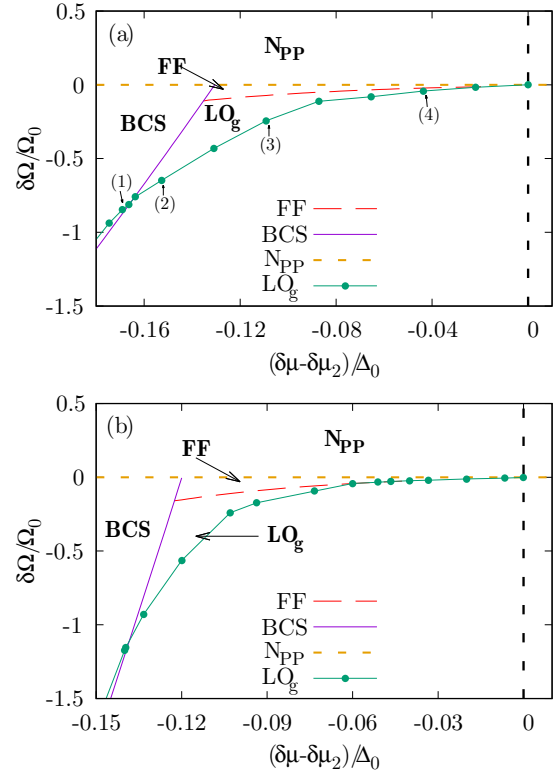

FIG. 8. The zero-temperature minima of FF, BCS, and LO_g thermodynamic potentials. The upper panel (a) is for interaction strength $\varepsilon_B = 0.10\varepsilon_F$ and panel (b) is for interaction $\varepsilon_B = 0.25\varepsilon_F$. The critical chemical-potential imbalance, $\delta\mu_2$ denotes the LO_g to N_{PP} transition and Δ_0 is the BCS energy gap at zero temperature. The thermodynamic potentials are defined with respect to the free Fermi gas thermodynamic potential, Ω_{free}, and scaled by the constant $\Omega_0 = 2\pi \times 10^{-3} N\varepsilon_F$. In panel (a), the labels from (1) to (4) refer to Fig. 9 and denote the configurations for which we studied the shape of the thermodynamic potential itself.

by a single point only. It is possible to increase the binding energy and thereby to relatively improve the accuracy of the calculation. As shown in Fig. 9(e), at $\varepsilon_B = 0.35\varepsilon_F$, the local maximum at low Q becomes more evident. Considering the accuracy of our numerical calculations and also the difficulty of reaching convergence close to the BCS-LO_g transition line, we cannot make a conclusive determination of the order of the BCS-LO_g transition. Throughout the work, we interpret it as a *weak* first-order transition, to reflect the fact that the structure of the local maximum is weak.

C. Finite temperature

We can extend the BdG equations from the zero-temperature regime to study the LO_g phase at finite temperatures. In the deep-BCS limit, the critical transition temperature, T_c^{BCS}, can be approximated from the gap equation in 2D, following the Landau theory of the second-order phase transition,

$$T_c^{\text{BCS}} \simeq \frac{2}{\pi} e^{\gamma - \ln(k_F a_{2D})} T_F, \tag{56}$$

where γ is the Euler–Mascheroni constant. We can estimate the tricritical-point (TCP) temperature, where the BCS, CC limit,
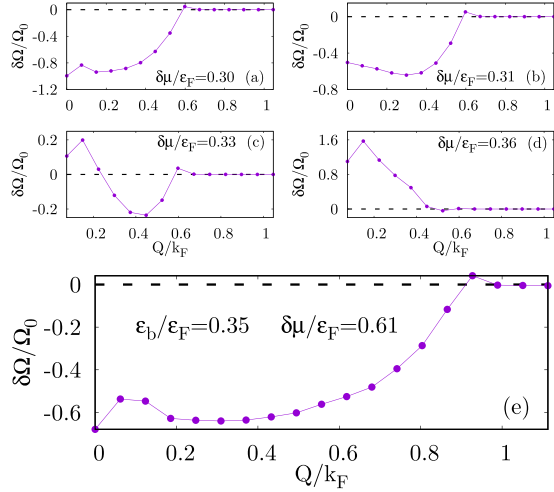
FIG. 9. The thermodynamic potential as a function of Q for interaction strength $\varepsilon_B = 0.1\varepsilon_F$ and chemical-potential difference (a) $\delta\mu = 0.3$, (b) $\delta\mu = 0.31$, (c) $\delta\mu = 0.33$, and (d) $\delta\mu = 0.36$. The plots (a)–(d) correspond to points (1)–(4), respectively, in Fig. 8(a). (e) BCS-LO$_g$ transition at higher binding energy $\varepsilon_B = 0.35\varepsilon_F$ to emphasize the first-order nature of the transition. The thermodynamic potential is defined with respect to the free Fermi gas through $\delta\Omega = \Omega - \Omega_{\text{free}}$, and scaled by a constant, $\Omega_0 = 2\pi \times 10^{-3} N\varepsilon_F$.

and FFLO phase intersect, with the numerical value [58–60]

$$T_{\text{TCP}} \simeq 0.561 T_c^{\text{BCS}}. \tag{57}$$

From our self-consistent BdG equations we plot out the phase diagram for the critical temperature as a function of chemical-potential difference in Fig. 10 for interaction strengths $\varepsilon_B = 0.10\varepsilon_F$ [Fig. 10(a)] and [Fig. 10(b)] $\varepsilon_B = 0.25\varepsilon_F$, the inset shows the entire phase diagram. The transition between the BCS and N_{PP} phase, found through the BCS theory, is second order for temperatures above T_{TCP}. The first-order CC limit (dashed line) is entirely contained in between the two LO$_g$ transition temperatures at any relevant $\delta\mu$ value. Moreover, the order of the phase transitions is preserved, the second-order phase transition between the LO$_g$ and N_{PP} phase is unaffected by an increasing temperature below TCP. The weak first-order BCS LO$_g$ is preserved within our numerical accuracy.

We note that, in the weakly interacting regime $\varepsilon_B = 0.10\varepsilon_F$, T_c^{BCS} is approximately $0.25T_F$. It appears that the mean-field treatment requires a beyond-mean-field approach to take into account the fact there is no superfluid behavior above the Berezinskii–Kosterlitz-Thouless (BKT) temperature $T_{\text{BKT}} \simeq 0.125T_F$. We observe that most of the LO$_g$ phase is below T_{BKT}, and within our numerical calculations the existence and availability of the LO$_g$ phase at finite temperatures is also below the TCP temperature, at least in the weakly interacting regime. However, we cannot provide accurate quantitative results for the transition temperatures among the phases under investigation due to the mean-field nature of the calculation.

V. SUPERFLUID DENSITY OF LO$_g$ PHASE

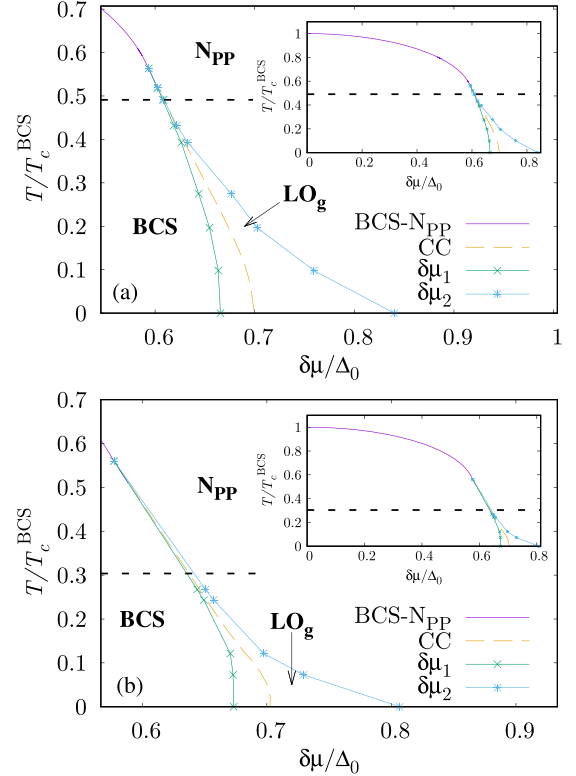The superfluid density is an essential signature of a superfluid system, and as we have seen the structure of the

FIG. 10. Critical temperature of the second-order BCS-N_{PP} (solid) transition, the CC limit (dashed), weak first-order BCS-LO$_g$ transition through $\delta\mu_1(T)$ (crosses), and second-order LO$_g$ N_{PP} through $\delta\mu_2(T)$ (stars). The graph is scaled with respect to the BCS critical temperature T_c^{BCS} at $\delta\mu = 0$ and the BCS pairing gap at zero temperature Δ_0. The inset shows the full phase diagram and the black dashed line is the BKT transition temperature.

pairing order parameter has been significantly altered for a finite polarization. We can study the superfluid density of a Fermi gas by imposing a superfluid twist [61–64]. The superfluid part of the system, if it exists, cannot react to small excitations like a normal gas and creates a superfluid current, whose magnitude is proportional to the superfluid density contained in the gas [65]. We impose the twist by modifying the pairing order parameter in Eq. (21),

$$\Delta(\mathbf{x}) = \Delta(\mathbf{x})e^{i\mathbf{Q}_s \cdot \mathbf{x}}, \tag{58}$$

where the twist momentum is $\mathbf{Q}_s$ and the superfluid velocity $\mathbf{v}_s$ is given by

$$\mathbf{v}_s = \frac{\mathbf{Q}_s}{2m}. \tag{59}$$

The Helmholtz free energy F must increase if we impose a flow in the superfluid phase and the shape of the free energy for small twists is shown to behave like the square of the phase twist amplitude around the point $F(\mathbf{Q}_s = \mathbf{0})$ [61],

$$\frac{F(\mathbf{Q}_s) - F(\mathbf{0})}{V} \simeq \frac{|\mathbf{Q}_s|^2}{2V}\left(\frac{\partial^2 F(\mathbf{Q}_s)}{\partial|\mathbf{Q}_s|^2}\right)_{\mathbf{Q}_s \to \mathbf{0}} \equiv \frac{1}{2}\rho_s m v_s^2, \tag{60}$$
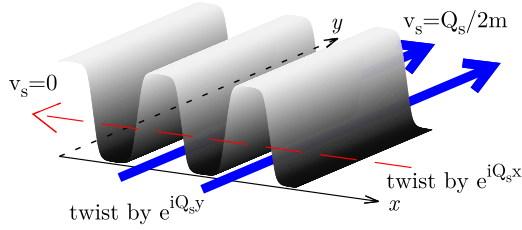
FIG. 11. Effect of a phase twist imposed on the pairing order parameter. In the parallel direction (red broken line), superfluid current can hardly be produced, while in the perpendicular direction (blue line), superfluid current is allowed to flow, except the regions where the order parameter vanishes and the spin imbalance is high.

where the superfluid density ρ_s is

$$\rho_s = 4m \left(\frac{\partial^2 F(\mathbf{Q}_s)}{\partial |\mathbf{Q}_s|^2} \right)_{\mathbf{Q}_s = 0}, \tag{61}$$

and the normal part density must be $\rho_n = n - \rho_s$.

Due to the symmetry we have imposed on the LO$_g$ order parameter and from Fig. 3, where the local spin polarization is peaked when $\Delta(\mathbf{x})$ vanishes, we can infer the fundamental properties of the superfluid phase. In Fig. 11, we illustrate the idea of what might happen when we impose a superfluid twist that is either parallel (x direction) or perpendicular (y direction) to the LO order parameter. A macroscopic current along the x direction must cross regions where the LO$_g$ phase has domain walls and thus cannot flow. A superfluid current along the y direction is able to flow as the order parameter is nonzero. By setting $\mathbf{Q}_s = Q_s \hat{\mathbf{x}}$, we find that there is no detectable superfluid density within our numerical precision. Thus, we restrict the following analysis to the perpendicular case, choosing $\mathbf{Q}_s = Q_s \hat{\mathbf{y}}$ and computing the superfluid density via Eq. (61) through a modification of the BdG equations given in Sec. III.

Equations (31) in the presence of the twist are now complex valued and need to be recast in a real-valued form. To achieve this we have to consider again the Heisenberg equations of motion and perform a new Bogoliubov transformation including the twist order parameter Eq. (58). The new modes will be decomposed as follows:

$$\psi_\uparrow(\mathbf{x}) = \sum_\eta \left[u_{\eta \mathbf{Q}_s \uparrow}(\mathbf{x}) c_{\eta \mathbf{Q}_s \uparrow} e^{-i E_{\eta \mathbf{Q}_s \uparrow} t} - v_{\eta \mathbf{Q}_s \downarrow}^*(\mathbf{x}) c_{\eta \mathbf{Q}_s \downarrow}^\dagger e^{i E_{\eta \mathbf{Q}_s \downarrow} t} \right],$$

$$\psi_\downarrow^\dagger(\mathbf{x}) = \sum_\eta \left[u_{\eta \mathbf{Q}_s \downarrow}^*(\mathbf{x}) c_{\eta \mathbf{Q}_s \downarrow}^\dagger e^{i E_{\eta \mathbf{Q}_s \downarrow} t} + v_{\eta \mathbf{Q}_s \uparrow}(\mathbf{x}) c_{\eta \mathbf{Q}_s \uparrow} e^{-i E_{\eta \mathbf{Q}_s \uparrow} t} \right],$$

$$\tag{62}$$

yielding

$$M_\uparrow \begin{bmatrix} u_{\eta \mathbf{Q}_s \uparrow} \\ v_{\eta \mathbf{Q}_s \uparrow} \end{bmatrix} = \begin{bmatrix} -\nabla_{\mathbf{x}}^2 - \mu_\uparrow & -\Delta(\mathbf{x}) e^{i \mathbf{Q}_s \cdot \mathbf{x}} \\ -\Delta(\mathbf{x})^* e^{-i \mathbf{Q}_s \cdot \mathbf{x}} & \nabla_{\mathbf{x}}^2 + \mu_\downarrow \end{bmatrix} \begin{bmatrix} u_{\eta \mathbf{Q}_s \uparrow} \\ v_{\eta \mathbf{Q}_s \uparrow} \end{bmatrix}. \tag{63}$$

We can remove the phase from the order parameter through the transformation $A M_\uparrow A^*$, where

$$A = \begin{bmatrix} e^{\frac{i}{2} \mathbf{Q}_s \cdot \mathbf{x}} & 0 \\ 0 & e^{-\frac{i}{2} \mathbf{Q}_s \cdot \mathbf{x}} \end{bmatrix}. \tag{64}$$

As in the derivation of the FFLO BdG equations, the two spin components are related through a unitary transformation and we only need to study one spin component. We thus define $u_{\eta \mathbf{Q}_s \uparrow} = u_{\eta \mathbf{Q}_s}$ and $v_{\eta \mathbf{Q}_s \uparrow} = v_{\eta \mathbf{Q}_s}$, obtaining the following form for the BdG equations,

$$\begin{bmatrix} -\left(\vec{\nabla} + i\frac{\mathbf{Q}_s}{2}\right)^2 - \mu_\uparrow & -\Delta(\vec{x}) \\ -\Delta(\vec{x}) & \left(\vec{\nabla} - i\frac{\mathbf{Q}_s}{2}\right)^2 + \mu_\downarrow \end{bmatrix} \begin{bmatrix} u_{\eta \mathbf{Q}_s} \\ v_{\eta \mathbf{Q}_s} \end{bmatrix}$$

$$= E_\eta^{\mathbf{Q}_s} \begin{bmatrix} u_{\eta \mathbf{Q}_s} \\ v_{\eta \mathbf{Q}_s} \end{bmatrix}. \tag{65}$$

Choosing a Hilbert basis of complex-valued functions,

$$\phi_{\mathbf{k}}(\mathbf{x}) = \frac{e^{i\mathbf{k} \cdot \mathbf{x}}}{\sqrt{V}}, \quad \mathbf{k} = \frac{2\pi}{\sqrt{V}} \mathbf{n},$$

with $\mathbf{n} \in \mathbb{Z}^2$, we expand the quasiparticle wave functions as

$$u_{\eta \mathbf{Q}_s} = \sum_{\mathbf{k}} A_{\mathbf{k}}^{(\eta \mathbf{Q}_s)} \phi_{\mathbf{k}}, \quad v_{\eta \mathbf{Q}_s} = \sum_{\mathbf{k}} B_{\mathbf{k}}^{(\eta \mathbf{Q}_s)} \phi_{\mathbf{k}},$$

and expand the BdG equations with the requirement that $\Delta(\mathbf{x})$ be a real valued, uni-directional function and a superposition of cosine Fourier modes. As in Sec. III, we obtain a block-diagonal set of matrix equations in n_2, giving

$$\begin{bmatrix} \varepsilon_{nm}^\uparrow & -\Delta_{n_1 m_1} \\ -\Delta_{nm} & -\varepsilon_{nm}^\downarrow \end{bmatrix} \begin{bmatrix} A_m^{(\eta \mathbf{Q}_s n_2)} \\ B_m^{(\eta \mathbf{Q}_s n_2)} \end{bmatrix} = E_\eta^{\mathbf{Q}_s n_2} \begin{bmatrix} A_n^{(\eta \mathbf{Q}_s n_2)} \\ B_n^{(\eta \mathbf{Q}_s n_2)} \end{bmatrix}, \tag{66}$$

where we define the two single-particle energies

$$\varepsilon_{nm}^\uparrow = \left[\left(\mathbf{k} + \frac{\mathbf{Q}_s}{2} \right)^2 - \mu_\uparrow \right] \delta_{nm},$$

$$\varepsilon_{nm}^\downarrow = \left[\left(\mathbf{k} - \frac{\mathbf{Q}_s}{2} \right)^2 - \mu_\downarrow \right] \delta_{nm}. \tag{67}$$

The order-parameter matrix elements are found from

$$\Delta_{nm} = \frac{1}{L} \int_{-L/2}^{L/2} dx \, \cos\left((n-m)x \right) \Delta(x). \tag{68}$$

The choice of the cutoff energy is matched to the $\mathbf{Q}_s = 0$ calculations and adjusted to ensure the calculation is independent from the cutoff choice.

In Fig. 12 we show the Helmholtz free energy under a phase twist $\mathbf{Q}_s = \mathbf{Q}_\perp = Q_s \hat{\mathbf{y}}$ with increasing twist amplitude (measured in units of the Fermi momentum k_F) at zero temperature and interaction strength $\varepsilon_B = 0.25\varepsilon_F$. The parabolic dependency in Q_s is obtained by fitting the data with polynomial cure, $ax^2 + bx^4$. We find the coefficient b is negligible and the coefficient a is then proportional to the superfluid density of the system using Eq. (61). We note that, in the presence of the LO order parameter, the calculation of the superfluid density becomes very difficult. The only way to increase the precision of our approach is to increase the size of the system, i.e., L. This can be done by increasing the number of particles; however, this greatly increases the computational cost. Previous computations related to the FF phase [66], which use similar methods, have been able to dramatically increase the accuracy of numerical calculations, approximately 10 times better than our accuracy.
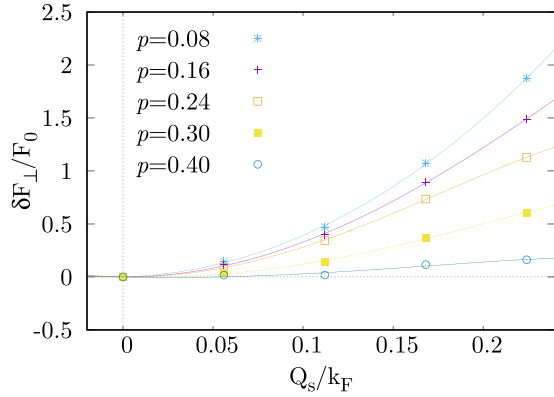
FIG. 12. The perpendicular Helmholtz free-energy difference $\delta F_\perp = F(\mathbf{Q}_\perp) - F(\mathbf{0})$ as a function of the phase twist, for various polarizations. The free-energy variation is calculated by using $\mathbf{Q}_\perp = Q_s \hat{y}$ and is plotted in units of a rescaling constant $F_0 = 2\pi \times 10^{-3} N \varepsilon_F$. The continuous lines are the data fit using a two-parameter polynomial curve $ax^2 + bx^4$.

In Fig. 13, we present the superfluid fraction as a function of the polarization at the interaction strength $\varepsilon_B = 0.25\varepsilon_F$ and at zero temperature. In general, we observe that an increase of polarization suppresses the superfluid density. As the LO momentum of the pairing gap increases with increasing polarization, as shown in Fig. 3(c), the local spin imbalance becomes more spread in space, making it more difficult for the superfluid current to flow. We note that there is a significant drop in the superfluid density for polarization larger than $p \simeq 0.4 p_{c2}$. This behavior may be due to the high polarization causing the pairing order parameter to be highly oscillatory, where the LO_g and LO_1 phases are matching, increasing the number of zeros in the order parameter and preventing the superfluid current from flowing. As a result, the superfluid fraction decreases dramatically, making this regime difficult to experimentally probe.

A direct observation of the superfluid density is available through the detection and measurement of excitations caused by resonant interactions on the gas. Although experimentally hard to probe, the propagation of second sound is a technique that has been successfully adopted to investigate the ratio n_s/n in a 1D Fermi gas [67], promoting this quantity as a viable experimental candidate to study Fig. 13.

VI. CONCLUSIONS

We have studied in detail the mean-field theory of a two-component 2D atomic Fermi gas in the presence of spin-population imbalance. The pairing order parameter has been self-consistently determined through numerical solutions of the BdG equations in the case of an s-wave scattering contact potential, allowed only between opposite-spin particles. We have considered different types of pairing order parameter and explored the phase transitions and the superfluid nature of the system. In particular, the LO *Ansatz* for the pairing order parameter has been refined and treated with reasonable approximations in order to make computations accessible and useful. In contrast to the previous studies with a FF *Ansatz* [37,38], such a refinement reveals the pivotal importance of the LO_g *Ansatz* among the broad FFLO family in 2D. The LO_g phase turns out to be energetically favorable with respect to both the FF and the original LO *Ansatz*.

The detection of the LO_g phase, similarly to the LO_1 case [68], is related to the density of states, otherwise called the LO phase signature. The Hamiltonian spectrum in the BCS phase must display a gap between states with positive and negative energies. In particular, the density of states must vanish in the energy interval $|E| < \Delta_{BCS}$. The presence of weakly bound Andreev states populates the gap with extra additional peaks due to the modulation in frequency of the order parameter Δ_{LO_g}. While the LO_1 phase has a single peak, multiple peaks are indeed expected to appear in the band gap in the LO_g case due to the frequency spectra of Fig. 4. This signature has been recently tested with promising results in probing the existence of the FFLO family [69].

The superfluid density of the LO_g phase has been calculated by adding a phase twist to the pairing order parameter. We have predicted the qualitative behavior of the superfluid density with increasing spin polarization.

The mathematical and computational methods employed in our work are satisfactory, although they are incomplete for providing exact quantitative results. Many of the configurations under investigation mimic some experimental settings for 2D or quasi-2D Fermi gases [45]. Therefore, we anticipate that our results might be useful for possible experimental realizations of a FFLO phase in 2D in the near future. We note also that a beyond-mean-field treatment is required to obtain quantitative results and to estimate the critical temperature of the LO_g phase.
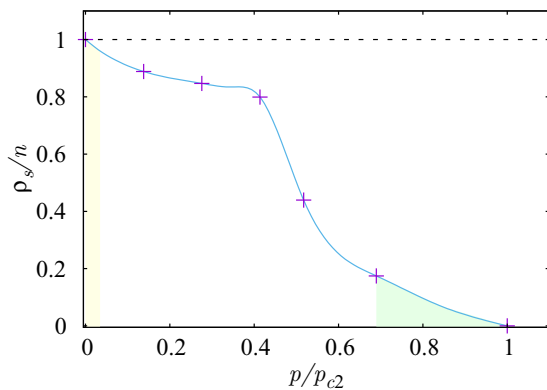

FIG. 13. The superfluid fraction ρ_s/n as a function of the polarization p at $\varepsilon_B = 0.25\varepsilon_F$ at zero temperature. The polarization is rescaled by the critical polarization $p_{c2} = 0.58$, at which the LO_g-N_{PP} transition occurs. The green and yellow regions correspond to the $LO_g \to LO_1$ and BCS regions shown in Fig. 2, respectively. The solid line is a guide line.

[1] D. D. Osheroff, R. C. Richardson, and D. M. Lee, Phys. Rev. Lett. **28**, 885 (1972).

[2] D. D. Osheroff, W. J. Gully, R. C. Richardson, and D. M. Lee, Phys. Rev. Lett. **29**, 920 (1972).

[3] A. J. Leggett, Phys. Rev. Lett. **29**, 1227 (1972).

[4] P. Fulde and R. A. Ferrell, Phys. Rev. **135**, A550 (1964).

[5] A. I. Larkin and Y. N. Ovchinnikov, Sov. Phys. JETP **20**, 762 (1965).

[6] J. Bardeen, L. N. Cooper, and J. R. Schrieffer, Phys. Rev. **108**, 1175 (1957).

[7] F. Steglich, R. Modler, P. Gegenwart, M. Deppe, M. Weiden, M. Lang, C. Geibel, T. Lühmann, C. Paulsen, J. Tholence, Y. Ōnuki, M. Tachiki, and S. Takahashi, Physica C (Amsterdam, Neth.) **263**, 498 (1996).

[8] M. Tachiki, T. Koyama, and S. Takahashi, Physica C (Amsterdam, Neth.) **263**, 1 (1996).

[9] A. Bianchi, R. Movshovich, C. Capan, P. G. Pagliuso, and J. L. Sarrao, Phys. Rev. Lett. **91**, 187004 (2003).

[10] R. Lortz, Y. Wang, A. Demuer, P. H. M. Böttger, B. Bergk, G. Zwicknagl, Y. Nakazawa, and J. Wosnitza, Phys. Rev. Lett. **99**, 187002 (2007).

[11] B. Bergk, A. Demuer, I. Sheikin, Y. Wang, J. Wosnitza, Y. Nakazawa, and R. Lortz, Physica C (Amsterdam, Neth.) **470**, S586 (2010).

[12] R. Casalbuoni and G. Nardulli, Rev. Mod. Phys. **76**, 263 (2004).

[13] M. W. Zwierlein, C. H. Schunck, A. Schirotzek, and W. Ketterle, Nature (London) **442**, 54 (2006).

[14] Y. Shin, M. W. Zwierlein, C. H. Schunck, A. Schirotzek, and W. Ketterle, Phys. Rev. Lett. **97**, 030401 (2006).

[15] D. E. Sheehy and L. Radzihovsky, Phys. Rev. Lett. **96**, 060401 (2006).

[16] L. Radzihovsky and D. E. Sheehy, Rep. Prog. Phys. **73**, 076501 (2010).

[17] S. Inouye, M. R. Andrews, J. Stenger, H.-J. Miesner, D. M. Stamper-Kurn, and W. Ketterle, Nature (London) **392**, 151 (1998).

[18] C. Chin, R. Grimm, P. Julienne, and E. Tiesinga, Rev. Mod. Phys. **82**, 1225 (2010).

[19] M. Greiner, O. Mandel, T. Esslinger, T. W. Hänsch, and I. Bloch, Nature (London) **415**, 39 (2002).

[20] I. Bloch, Nat. Phys. **1**, 23 (2005).

[21] M. Veillette, E. G. Moon, A. Lamacraft, L. Radzihovsky, S. Sachdev, and D. E. Sheehy, Phys. Rev. A **78**, 033614 (2008).

[22] X.-J. Liu and H. Hu, Phys. Rev. A **87**, 051608 (2013).

[23] F. Wu, G.-C. Guo, W. Zhang, and W. Yi, Phys. Rev. Lett. **110**, 110401 (2013).

[24] C. Mora and R. Combescot, Phys. Rev. B **71**, 214504 (2005).

[25] T. Mizushima, K. Machida, and M. Ichioka, Phys. Rev. Lett. **95**, 117003 (2005).

[26] Z. Cai, Y. Wang, and C. Wu, Phys. Rev. A **83**, 063621 (2011).

[27] W. V. Liu and F. Wilczek, Phys. Rev. Lett. **90**, 047002 (2003).

[28] G. Sarma, J. Phys. Chem. Solids **24**, 1029 (1963).

[29] S.-T. Wu and S. Yip, Phys. Rev. A **67**, 053603 (2003).

[30] C.-H. Pao, S.-T. Wu, and S.-K. Yip, Phys. Rev. B **73**, 132506 (2006).

[31] P. F. Bedaque, H. Caldas, and G. Rupak, Phys. Rev. Lett. **91**, 247002 (2003).

[32] T. K. Koponen, T. Paananen, J.-P. Martikainen, and P. Törmä, Phys. Rev. Lett. **99**, 120403 (2007).

[33] T. K. Koponen, T. Paananen, J.-P. Martikainen, M. R. Bakhtiari, and P. Törmä, New J. Phys. **10**, 045014 (2008).

[34] M. J. Wolak, B. Grémaud, R. T. Scalettar, and G. G. Batrouni, Phys. Rev. A **86**, 023630 (2012).

[35] X.-J. Liu, H. Hu, and P. D. Drummond, Phys. Rev. A **76**, 043605 (2007).

[36] Y. an Liao, A. S. C. Rittner, T. Paprotta, W. Li, G. B. Partridge, R. G. Hulet, S. K. Baur, and E. J. Mueller, Nature (London) **467**, 567 (2010).

[37] G. J. Conduit, P. H. Conlon, and B. D. Simons, Phys. Rev. A **77**, 053617 (2008).

[38] D. E. Sheehy, Phys. Rev. A **92**, 053631 (2015).

[39] K. Machida and H. Nakanishi, Phys. Rev. B **30**, 122 (1984).

[40] J. E. Baarsma and P. Törmä, J. Mod. Opt. **63**, 1795 (2016).

[41] S. Yin, J.-P. Martikainen, and P. Törmä, Phys. Rev. B **89**, 014507 (2014).

[42] P. A. Murthy, I. Boettcher, L. Bayha, M. Holzmann, D. Kedar, M. Neidig, M. G. Ries, A. N. Wenz, G. Zürn, and S. Jochim, Phys. Rev. Lett. **115**, 010401 (2015).

[43] W. Ong, C. Cheng, I. Arakelyan, and J. E. Thomas, Phys. Rev. Lett. **114**, 110403 (2015).

[44] K. Fenech, P. Dyke, T. Peppler, M. G. Lingham, S. Hoinka, H. Hu, and C. J. Vale, Phys. Rev. Lett. **116**, 045302 (2016).

[45] P. Dyke, K. Fenech, T. Peppler, M. G. Lingham, S. Hoinka, W. Zhang, S.-G. Peng, B. Mulkerin, H. Hu, X.-J. Liu, and C. J. Vale, Phys. Rev. A **93**, 011603 (2016).

[46] N. Yoshida and S.-K. Yip, Phys. Rev. A **75**, 063601 (2007).

[47] A. Bulgac and M. McNeil Forbes, Phys. Rev. Lett. **101**, 215301 (2008).

[48] J. E. Baarsma and H. T. C. Stoof, Phys. Rev. A **87**, 063612 (2013).

[49] D. S. Petrov and G. V. Shlyapnikov, Phys. Rev. A **64**, 012706 (2001).

[50] J. Levinsen and M. M. Parish, Strongly interacting two-dimensional Fermi gases, in *Annual Review of Cold Atoms and Molecules* (World Scientific Pub Co Pte Lt, 2015), Chap. 1, pp. 1–75.

[51] X.-J. Liu, H. Hu, and P. D. Drummond, Phys. Rev. A **75**, 023614 (2007).

[52] It is possible the ground state for these polarizations is the more complicated LO_2 phase, which is not considered in this work.

[53] I. Boettcher, L. Bayha, D. Kedar, P. A. Murthy, M. Neidig, M. G. Ries, A. N. Wenz, G. Zürn, S. Jochim, and T. Enss, Phys. Rev. Lett. **116**, 045303 (2016).

[54] The distinction between the fully polarized normal Fermi gas N_{FP} and the partially polarized N_{PP} that occurs when $\delta\mu > \mu$ is not taken into account here and we will use the notion of free Fermi gas for the N_{PP} phase.

[55] L. He and P. Zhuang, Phys. Rev. A **78**, 033613 (2008).

[56] M. M. Parish, F. M. Marchetti, A. Lamacraft, and B. D. Simons, Nat. Phys. **3**, 124 (2007).

[57] The FF line of minima is always above the LO_g line close to the BCS line, although at high $\delta\mu$ values, the model accuracy does not allow us to conclude whether there is, or is not, another transition FF-LO_g. Besides, we must say that is very inessential because, at high $\delta\mu$, the energy-gap parameter reduces continuously its amplitude until it vanishes and the difference between the magnitude of the two *Ansätze* might be negligible. Moreover, at high $\delta\mu$ values it's even more likely,

as discussed in Sec. II, the presence of an LO_2 phase. The latter might actually be favourable with respect to both FF and LO_g.

[58] H. Burkhardt and D. Rainer, Ann. Phys. (Berlin, Ger.) **506**, 181 (1994).

[59] S. Matsuo, S. Higashitani, Y. Nagato, and K. Nagai, J. Phys. Soc. Jpn. **67**, 280 (1998).

[60] R. Combescot and C. Mora, Eur. Phys. J. B **28**, 397 (2002).

[61] E. Taylor, A. Griffin, N. Fukushima, and Y. Ohashi, Phys. Rev. A **74**, 063626 (2006).

[62] N. Fukushima, Y. Ohashi, E. Taylor, and A. Griffin, Phys. Rev. A **75**, 033609 (2007).

[63] E. Taylor, Phys. Rev. B **77**, 144521 (2008).

[64] M. Holzmann and G. Baym, Phys. Rev. B **76**, 092502 (2007).

[65] M. E. Fisher, M. N. Barber, and D. Jasnow, Phys. Rev. A **8**, 1111 (1973).

[66] Y. Cao, X.-J. Liu, L. He, G.-L. Long, and H. Hu, Phys. Rev. A **91**, 023609 (2015).

[67] L. A. Sidorenkov, M. K. Tey, R. Grimm, Y.-H. Hou, L. Pitaevskii, and S. Stringari, Nature (London) **498**, 78 (2013).

[68] Y. L. Loh and N. Trivedi, Phys. Rev. Lett. **104**, 165302 (2010).

[69] H. Mayaffre, S. Krämer, M. Horvatić, C. Berthier, K. Miyagawa, K. Kanoda, and V. F. Mitrović, Nat. Phys. **10**, 928 (2014).